Influence of Surface-Initiated Polymerization Rate and Initiator Density on the Properties of Polymer Brushes

Hong Liu,[†] Min Li,[‡] Zhong-Yuan Lu,*[,†] Zuo-Guang Zhang,[‡] and Chia-Chung Sun[†]

Institute of Theoretical Chemistry, State Key Laboratory of Theoretical and Computational Chemistry, Jilin University, Changchun 130023, China, and Key Laboratory of Aerospace Materials and Performance (Ministry of Education), School of Materials Science and Engineering, Beihang University, Beijing 100083, China

Received December 18, 2008; Revised Manuscript Received February 17, 2009

ABSTRACT: The surface-initiated polymerization with different initiator densities and different polymerization rates is investigated using molecular dynamics simulation method. We find that the initiator density, together with the polymerization rate, greatly determines the polymer brush structure, the initiation efficiency, and the graft density, especially when the initiator density is high. The excluded volume effect also plays a crucial role in the system when the chains are densely grafted. By tuning the initiator density and modifying the polymerization rate, we can obtain the polymer brushes with different degrees of polydispersity. This study partially emphasizes the importance of considering the effects of polymerization rate in further investigations.

1. Introduction

Polymer brushes are generally defined as layers of polymer chains end-grafted to a surface. They give rise to a wide range of important technological and industrial applications, such as lubrications, oil recovery, colloid stability, modification of surfaces, adhesion, reversible tuning of wetting, biotechnology, and contact formation.[1−5] A number of polymerization mechanisms are provided for the preparation of polymer brushes,[6] such as free-radical,[7] cationic,[8] ring-opening metathesis polymerization,[9] atom-transfer free-radical polymerization (ATRP),[10−14] polymerization using 2,2,6,6-tetramethyl-1-piperidyloxy,[15] anionic polymerization,[16] and reversible addition−fragmentation and transfer polymerization.[17,18]

In recent years, a large amount of research[4,5,10,11,19−46] has been carried out that focuses on polymer brushes with different graft densities. Alexander[19] and de Gennes[20] had theoretically demonstrated that the polymer chains tend to be strongly stretched along the direction perpendicular to the graft substrate when the graft density is high. Other researchers also pointed out that the polymer brushes will exhibit completely different conformations in solvent as the graft density is varied.[47,48] In the case of low graft densities, the "mushroom" chain conformation similar to that of the free chains will appear for the end-tethered chains. With increasing graft density, the chains are stretched to form the "forest" of polymer brushes because the repulsive interactions will drastically increase with increasing graft density.[49]

It is also important to study the effects of polymerization rate on the properties of polymer brushes. Prucker and Rühe[50] experimentally illustrated that the activation of initiator and the diffusion of monomers to the reactive sites are the primary factors that affect the surface-initiated polymerization. They pointed out that by decreasing the probability of deactivation of the polymer radicals in ATRP, it is possible to control the layer thickness; also, if the polymerization conditions are altered in such a way, higher molecular weights will be obtained. Wittmer et al.[51] indicated in their theoretical research that the brush chains are strongly extended from the surface but extremely polydisperse because the longer chains will grow up from the layer of compact short chains to catch the outer abundant free monomers. A basic assumption in their research is that many simultaneously growing chains compete for the small influx of monomers to the surface.

However, simulation studies of such systems scarcely covered the effects of polymerization rate. Matyjaszewski et al.[52] and Milchev et al.[53] carried out simulation studies focusing on the chain length and the graft density distributions of surface-initiated polymerization taking into account the living chains with activation/deactivation processes and without termination. The simulation results of Matyjaszewski et al.[52] suggested broader molecular weight and chain end distributions of the polymer brushes. Milchev et al.[53] pointed out that when the initiator density is high, the molecular weight distribution in the equilibrium polymer brushes obeys an $N^{-7/4}$ power law. Moreover, Xiao and Wirths[54] and Kim et al.[55] had extended kinetic simulations with activation/deactivation equilibrium and termination in the model, and they predicted the graft mount for surface-initiated ATRP as the time elapses.

Regarding the effects of polymerization rate (and most importantly, its interplay with the initiator density) on the properties of the polymer brushes, here we present a new simulation study on the surface-initiated polymerization process by utilizing a reasonably physical model similar to that in ref 53 but taking into consideration the variation of polymerization rates in the simulations. We find that the properties of polymer brushes are greatly dependent on the coupling between the initiator density and the initiation efficiency, which, however, is related to the former and the polymerization rate to a large extent. Here the initiation efficiency is defined as the ratio of the number of saturated initiators to the total number of initiators. However, the exclude volume effect plays a crucial role in such system, especially when the chains are densely grafted. As a result, in the system with higher initiator density and lower polymerization rate, the grafted chains tend to choose the conformation that greatly stretched in the direction perpendicular to the surface. By tuning the initiator density and choosing different polymerization rates, we can obtain the polymer brushes with different degrees of polydispersity.

The article is organized as follows: Section 2 exhibits the simulation details, Section 3 shows the results and the corre-

* Corresponding author. E-mail: luzhy@jlu.edu.cn. Tel: 0086 431 88498017. Fax: 0086 431 88498026.
[†] Jilin University.
[‡] Beihang University.

10.1021/ma802817r CCC: $40.75
Published on Web 03/18/2009

sponding discussion, and Section 4 presents the concluding remarks.

2. Model and Simulation Details

2.1. Truncated and Shifted Lennard-Jones Potential and Dissipative Particle Dynamics Thermostat. In this study, we consider the truncated and shifted Lennard-Jones (LJ) potential between the particles (also known as Weeks−Chandler−Andersen potential),[56] in which the potential vanishes at the cutoff radius ($r_c = 2^{1/6}$) so that only its repulsive part is left

$$U(r) = U_{LJ}(r) - U_{LJ}(r_c) \tag{1}$$

with

$$U_{LJ}(r) = 4\epsilon\left[\left(\frac{\sigma}{r}\right)^{12} - \left(\frac{\sigma}{r}\right)^{6}\right] \tag{2}$$

For simplicity, we define the units in the simulations by setting $m = 1$, $\sigma = 1$, and $\epsilon = 1$.

Polymer chains are constructed by connecting the neighboring monomers together via finite extensible nonlinear elastic (FENE) spring potential[57,58]

$$U_{FENE} = \begin{cases} -\frac{1}{2}kl_{max}^2 \ln[1 - (r/l_{max})^2], & (r < l_{max}) \\ \infty, & (r \geq l_{max}) \end{cases} \tag{3}$$

where the spring constant is $k = 10\epsilon/\sigma^2$, a little weaker than the value in ref 5, so that the influence of the pressure variation on the system caused by bonding chain segments is slight. Here $r = |\mathbf{r}_i - \mathbf{r}_j|$ is the distance between neighboring monomers. The longest stretch of the bonds l_{max} is chosen according to the condition of bond uncrossibility[59,60] that $2^{1/2}r_{min} > l_{max}$, where we obtain the exact minimal distance between two particles r_{min} from radial distribution function (RDF),[60] and then the choice of l_{max} is clear.

The dissipative particle dynamics (DPD) thermostat is employed here to control the constant temperature. In addition to the forces originated from LJ and FENE potentials, interparticle interactions also include pairwise dissipative and random forces. They are given by[61] $\mathbf{F}_{ij}^{D} = -\gamma\omega^{D}(r_{ij})(\mathbf{v}_{ij}\cdot\mathbf{e}_{ij})\mathbf{e}_{ij}$ and $\mathbf{F}ij^{R} = \sigma\omega^{R}(r_{ij})\xi_{ij}\Delta t^{-1/2}\mathbf{e}_{ij}$, where $\mathbf{r}_{ij} = \mathbf{r}_i - \mathbf{r}_j$, $r_{ij} = |\mathbf{r}_{ij}|$, $\mathbf{e}_{ij} = \mathbf{r}_{ij}/r_{ij}$, and $\mathbf{v}_{ij} = \mathbf{v}_i - \mathbf{v}_j$. ξ_{ij} is a random number with zero mean and unit variance. The noise level is taken to be $\sigma = 3$ according to ref 61. The weight functions $\omega^{D}(r_{ij})$ and $\omega^{R}(r_{ij})$ of the dissipative and random forces couple together to form a thermostat. Español and Warren[62] showed the correct relations between the two functions, $\omega^{D}(r) = [\omega^{R}(r)]^2$ and $\sigma^2 = 2\gamma k_B T$. Following ref 63, we take the form of $\omega^{D}(r)$ and $\omega^{R}(r)$ to be

$$\omega^{D}(r) = [\omega^{R}(r)]^2 = \begin{cases} [1 - (r/r_c)]^2 & (r < r_c) \\ 0 & (r \geq r_c) \end{cases} \tag{4}$$

DPD thermostat acting on an LJ system was evaluated as a potentially useful technique for controlling the temperature.[5,63] In ref 63, the authors chose a time step $\Delta t = 0.01$, and in ref 5, the authors chose smaller values: $\Delta t = 0.0005$ or 0.002. Here because of the existence of the walls in the simulations, we have to pursue a balance between the influence of heat/momentum dissipation caused by the walls on the temperature fluctuation and the control of temperature by the DPD thermostat. We thus find that $\Delta t = 0.005$ is a reasonable value in our simulation.

2.2. Model Construction. In this study, the model used to describe the surface-initiated polymerization is composed of free monomers and planar walls. The periodic boundary conditions (PBC) are applied in both x and y directions, but in the z direction, two layers of regularly arranged and densely packed frozen particles are utilized to form the wall. The interaction parameters between particles are set to be the same; that is, $\epsilon_{MM} = \epsilon_{MW} = \epsilon_{WW} = 1$, in which ϵ_{MM} denotes the repulsive strength between two monomers, ϵ_{MW} between a monomer and a wall particle and ϵ_{WW} between two wall particles. Some of the wall particles in the upper layer of the bottom wall are chosen to be the initiators so that the polymerization starts from the surface of the bottom wall to generate the end-tethered chains. The distance between the layers in a wall, d_L, is determined by the density of the wall particles, ρ_W; that is, $d_L = \rho_W^{-1/3}$. (ρ_W is a preset parameter, denoting the number of wall particles in unity volume, so d_L is the distance of the neighboring wall particles in the x, y, and z directions.) Because the interaction cutoff radius $r_c = 2^{1/6}$, the monomers are not able to feel the existence of the wall particles from the third layer, even if a finitely larger ρ_W (for example, $\rho_W = 7$) is chosen. Therefore, the impenetrable wall can be reasonably described by two closely packed layers of frozen wall particles.

In the simulations, the temperature is set equal to ϵ; that is, $k_B T = \epsilon = 1$. The particle density is kept as $\rho = 0.85$.[63] According to ref 63, the Schmidt number, S_c, in such a system is roughly $S_c \approx 30$, corresponding to a value for a real fluid. The reduced box size is $L_x = L_y = 16.837$, and $L_z = 56.123$. (The brushes are grafted from the bottom wall at $Z = -L_z/2 = -28.0615$, and the top wall is at $Z = L_z/2 = 28.0615$.) Therefore, the system consists of 13 523 particles. Here we choose a larger L_z compared with L_x and L_y so that there are relatively larger spaces for the polymer brushes to grow up, and thus we can observe the processes of fast polymerization even in a relatively long period.

2.3. Modeling the Polymerization. In the bottom wall, some orderly distributed initiating sites are selected that represent an initiator density σ_i, defined as $\sigma_i = N_i/(L_x \times L_y)$, where N_i denotes the number of initiators. Here we employ the idea in our previous model[64] by introducing the polymerization probability, P_r, to control the process of polymerization. In each reaction interval, τ, if an active end meets several monomers in the interaction radius, then it first randomly chooses one of the monomers as an reacting object. Subsequently, another random number is generated, and by checking if it is smaller than the preset P_r, we decide whether the monomer will connect with the active end. During polymerization, the newly connected monomers then turn to be the growth centers in the next propagation step of the same chain to connect other free monomers so that the active end is transferred forward. In this model, the chain termination step is omitted, which is the same as that in ref 65. It is easy to find that there is a specific relationship between the polymerization rate, r_p, and the reaction probability, P_r

$$r_p = -\frac{d[M]}{dt} = \frac{[P^*]P_r}{\tau} \tag{5}$$

where $[M]$ is the free monomer concentration, $[P^*]$ is the concentration of growth centers, and τ is the reaction time interval. Therefore, the model corresponds to the polymerization process with a constant reaction rate. In the simulations, we choose five typical values of P_r ($P_r = 0.0005$, 0.001, 0.002, 0.005, and 0.01) to study the effect of the polymerization rate on the properties of the polymer brushes. We assume that the different polymerization probabilities correspond to different polymerization rates of the systems determined by different levels of reaction activation energies.[64] Here $P_r = 0.01$ corresponds to a fast process of polymerization, and $P_r = 0.0005$ corresponds to a slow one. Because the polymerization can be

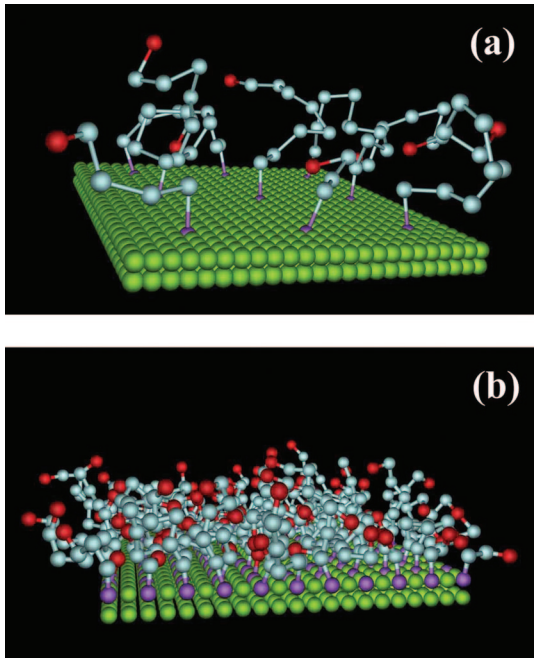

Figure 1. Snapshots of the surface-initiated polymerization with (a) a low initiator density $\sigma_i = 0.032$ and (b) a high initiator density $\sigma_i = 0.508$. The densely packed green beads represent the wall particles, the purple beads represent the initiators, the gray beads represent the grafted monomers, and the red beads represent the active ends of the chains. The free monomers are omitted here for clarity.

controlled under relatively low reaction rate in our model, it is not necessary to specially add the activation/deactivation process as in ATRP for the active ends. We consider the reversible activation process to be the fine details on the atomistic level inside the active ends of the chains, which can be reasonably ignored in our coarse-grained model. Although the general concept of living polymerization in the soft matter physics community often means reversible polymerization, here we reasonably ignore the concept difference and consider our model to be a kind of living because it is controllable under low reaction rate. This handling causes our model to be a little different from that of ref 53, in which the authors considered the reversible polymerization; that is, the end bonds of the chains have the probability of breaking, which is associated with a true Hamiltonian. Therefore, in that model, the system is in full equilibrium, both for the generalized coordinates and for the topology. Nevertheless, in our model, the chemical bonds of the chains correspond to essentially infinite energy gain. Therefore, it is a practically irreversible polymerization model. Different behavior should be expected for irreversible polymerization and reversible polymerization, as in ref 53. In the irreversible polymerization, the mass distribution is not at thermal equilibrium but is imposed by the dynamical pathway. Because of this, it can be hoped that very different brush structures might be synthesized.

Figure 1a shows the snapshot of the surface-initiated polymer chains with a low initiator density, $\sigma_i = 0.032$, in which only nine chains are grown up. The snapshot is obtained by extracting the grafted particle coordinates just a few time steps after the polymerization is originated so that the lengths of the chains are short. (The free monomers are eliminated in the Figure for clarity.) In comparison, Figure 1b exhibits the snapshot of the grown-up short chains with a higher initiator density $\sigma_i = 0.508$.

3. Results and Discussion

The simulations are conducted in canonical ensemble. The Groot-and-Warren-modified velocity Verlet algorithm is used

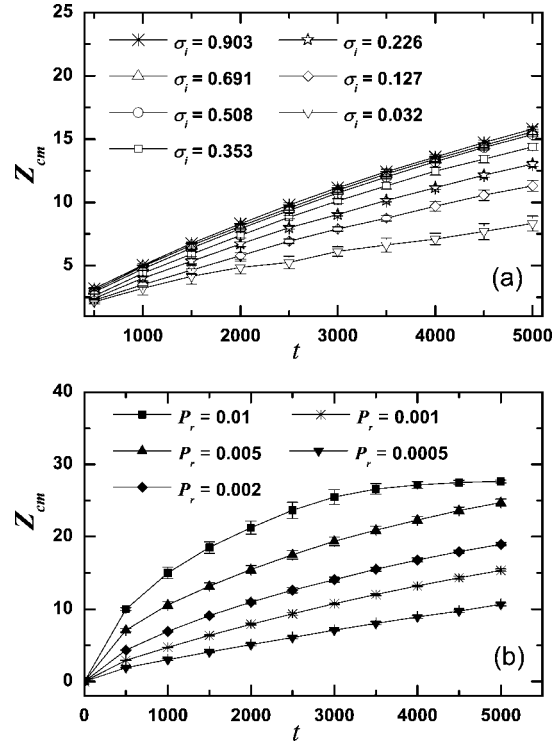

Figure 2. Time evolution of the distance of the center of mass of the grafted chains from the grafting plane (Z_{cm}) (a) with different σ_i at P_r= 0.001 and (b) with $\sigma_i = 0.508$ but different P_r. For each data point, four independent samples are simulated under the same condition to calculate Z_{cm} mean value and the error bar.

for numerical integration.[61] The initial configuration is set to be the randomly distributed free monomers in the system, then 1×10^5 steps molecular dynamics (MD) integration is carried out to relax the system. Consequently, a process of polymerization with 1×10^6 time steps is modeled. Here we choose the value of reaction time interval to be $\tau = 0.05$; that is, the polymerization of a specific active end may take place every 10 time steps depending on P_r because $\Delta t = 0.005$.

3.1. Controllability of Polymerization Process. A significant characteristic of living polymerization is that it is controllable; that is, during the polymerization process, the distance between the center of mass of the grafted chains and the grafting plane should increase linearly in the substrate normal direction. Therefore, we have checked our surface-initiated polymerization model on this issue. Figure 2a shows the time evolution of the distance between the center of mass of the grafted chains and the plane, Z_{cm}, with different σ_i at $P_r = 0.001$, which corresponds to a relatively slow polymerization rate (Here, Z_{cm} can also be considered to be the mean layer half-height of the film). It is clearly shown in Figure 2a that for the systems with different initiator densities, Z_{cm} exhibits an almost linear increase. The system with larger initiator density yields a larger increasing slope. In the case of such a slow reaction rate ($P_r = 0.001$), the competitions of the propagation between different chains are very weak. In other words, the ambient free monomers are abundant for the chains to propagate. However, it is reasonable to imagine that the growth behaviors of the systems with the same reaction rate but different initiator densities are different. In the case of low initiator densities, the tethered chain configuration is "mushroom"-like, whereas densely grafted chains will be obliged to grow nearly straight and form the forest of brushes. Therefore, the polymer brushes with larger values of σ_i exhibit higher increasing slope between Z_{cm} and time.

However, when we consider a faster reaction rate, the model polymerization will become slightly uncontrollable. Figure 2b

shows the time evolution of Z_{cm} of the grafted chains with $\sigma_i = 0.508$ but different P_r. It is obvious that in the systems with faster polymerization rates, the curves of $Z_{cm} \sim t$ deviate from the linear style more or less, showing the uncontrollable feature. The $Z_{cm} \sim t$ curve for $P_r = 0.01$ reaches a plateau with $Z_{cm} \approx 28.0615$ in the late stage of polymerization, implying that the center of mass of the polymer brushes is just at the middle between the two walls, namely, the brushes have completely filled in the simulation box. The slightly nonlinear part of each curve in the early stage is reasonable, during which the film of the polymer brushes is not yet formed, and only very short chains exist. Therefore, it is necessary to choose slow-to-moderate reaction rates in the model to keep it a controllable living polymerization and at the same time to guarantee the efficiency of polymerization. Therefore, for comparison in the following simulations, $P_r = 0.001$, 0.002, and 0.005 are chosen as the reaction probabilities of living polymerization to represent relatively slow, moderate, and fast reaction rates, respectively.

It should be specially stressed that $Z_{cm} \sim t$ does not increase linearly ideally, implying complex influences from possible factors such as the diffusion limited aggregation (DLA),[66,67] the relaxation of the brush chains, the screening effect of the grown chains on the unsaturated initiators, and so on. In the systems, only part of the free monomers participate in the polymerization, the relationship $Z_{cm} \sim t$ is expected to be dominantly governed by DLA.

3.2. Influence of Wall Roughness. In this model, we construct a wall by regularly arranging the densely packed and fixed wall particles in two planar layers. Therefore, it is not the type of idealized flat wall and the wall roughness is greatly dependent on the density of the wall particles, ρ_W. When we choose a larger value of ρ_W, we can obtain a smoother wall because the wall particles are more densely packed. However, it is simply unphysical if the neighboring particles are too close. However, to model different initiator densities, it is necessary to change the value ρ_W so that we can finely tune the number of wall particles to make the value σ_i reasonably represent the global initiator density of the surface without any local differences. Therefore, studying the influence of the wall roughness on the system is actually important. As a kind of neutral wall, its influence is only restricted to the polymer brushes or free monomers near the wall; that is, the walls with different ρ_W values may provide different repulsive strengths to the end-tethered polymer brushes so that the latter may exhibit different stretching degrees in the z direction only in a layer near the wall. Therefore, we use the second Legendre polynomial $P_2(\cos\theta_1) = [3\langle\cos^2\theta_1\rangle - 1]/2$ as a measure for checking the averaged first bond orientation of the polymer brushes,[5,53,68] which can be taken to be a criterion for the repulsive strength from the wall. Here θ_1 is defined as the angle between the first bond vector (connecting the anchoring initiator and the first grafted monomer) and the z axis. Therefore, $P_2 = -0.5$ denotes the bond orientation of lying parallel to the wall, $P_2 = 1$ represents the bonds lying perpendicular to the wall, and $P_2 = 0$ represents the bonds that are randomly oriented. Figure 3 shows the averaged first bond orientation of the polymer brushes with different ρ_W values. It is clearly shown in Figure 3 that when $\rho_W = 1$, the wall is too rough and cannot provide strong repulsion for the first grafted monomers of the polymer brushes. As a result, the averaged value of P_2 of the first bond is <0.5. When $\rho_W = 2$, the repulsive force from the wall is greatly enhanced, so we obtain a larger value of P_2. When $\rho_W \geq 3$, the value of P_2 does not change much with increasing ρ_W, which implies that the wall particles distributed around the anchoring site impose strong repulsive forces on the first grafted monomer from different directions, which makes the first bond have to choose the orientation that is nearly perpendicular to the surface.

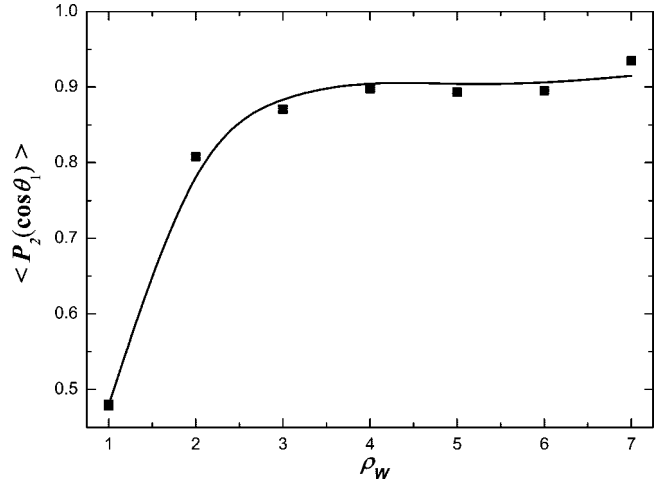

Figure 3. Averaged first bond orientation $\langle P_2(\cos\theta_1)\rangle$ of the polymer brushes with different ρ_W. Four independent samples are simulated under the same condition to calculate $\langle P_2(\cos\theta_1)\rangle$ and the error bar. The error bar size is smaller than the symbol size, so it is invisible. The solid line is drawn to guide the eye.

Therefore, we have adopted the walls with densities of $3 \leq \rho_W \leq 7$ in the simulations without biasing the polymer brush properties.

3.3. Initiator Density and the Graft Density. For polymer brushes, the number of grafted monomers should be greatly dependent on the initiator density σ_i on the surface. Therefore, the graft density, ρ_G, defined as $\rho_G = N_G/(L_x \times L_y)$, where N_G denotes the number of grafted monomers, should also be dependent on σ_i. Supposing that there is no excluded volume effect between the chains, more surface-anchored initiators should yield more grafted monomers within the same period of polymerization if the polymerization rates are the same. However, when the excluded volume effect is taken into account, the initiation efficiency becomes an important factor. Yamamoto et al.[10,45] applied the photodecomposition to change the initiator density and used the FT-IR method to estimate the graft density in the poly(methyl methacrylate) (PMMA) brushes, and then they observed an almost constant graft density when the initiator density is higher than a critical value.[45,69] They also pointed out that when the initiator density is lower than a critical value, the initiation efficiency is nearly 100%. Ma et al. also reported a similar relationship between σ_i and ρ_G in their experiments for oligo(ethylene glycol) methyl methacrylate polymerized on a Au-coated substrate with a mixed self-assembled monolayer.[46]

We have also studied the influence of the initiator density on the graft density in our simulations. Figure 4a shows the variation of the grafted monomer fraction (f_G) with increasing σ_i at different polymerization rates. Here we calculate the grafted monomer fraction f_G because $f_G = (\rho_G V)/N_T$, and V (the volume of the box) and N_T (the total number of the particles) are both constant. At different polymerization rates considered in our simulations, the relationship between f_G and σ_i is very similar to that reported in experiments.[10,45,69] Moreover, we find a window of σ_i that $\sigma_i = 0.353-0.508$ as the critical values of the initiation efficiency (except the curve with $P_r = 0.01$, which is proven to be an uncontrollable reaction). Each curve arrives at a plateau after the critical value, and the faster the reaction, the higher the plateau. It is easily understood that in the same period of polymerization, the faster reaction is able to graft more free monomers. In our simulations, the number of grafted monomers is thus dependent on the polymerization rate as well as the polymerization time. We have also compared the relationship between f_G and σ_i in different polymerization stages

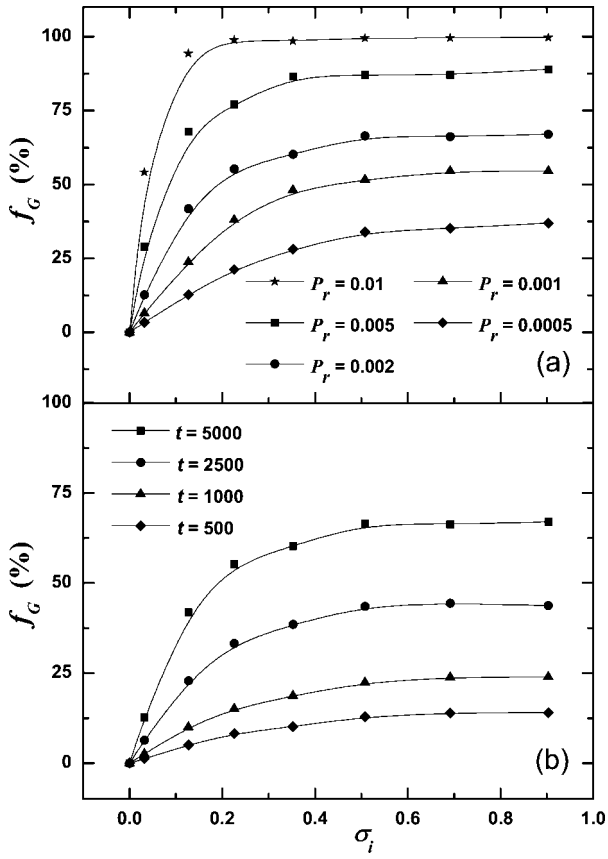

Figure 4. Variation of the grafted monomer fraction, f_G, with increasing σ_i (a) for the polymerization process with different rates and (b) in different polymerization stages with the same polymerization rate, $P_r = 0.002$.

of the systems with the same polymerization rate $P_r = 0.002$. (See Figure 4b.) It is obvious that f_G always increases with increasing σ_i, and f_G is larger for longer polymerization time. It should be noted that Jones et al. observed a nearly linear increase in the graft density with increasing σ_i in the experiment of PMMA brushes polymerized on an Au-coated mica, indicating that the surface causes poorer initiation efficiency.[11] However, in our simulations, the wall is a kind of simplified model with close-packing particles, ignoring the detailed intrinsic structures of different substrates. Therefore, we focus on only the general cases of surface-initiated polymerization without considering the surfaces with any special initiation efficiency in our simulations.

3.4. Graft Density Profiles. To characterize the film thickness and the structure of the polymer brushes, the graft density profile in the z direction is one of the most suitable physical properties. To present the dynamic process of the film growth, we plot the graft density profile in the z direction, $\rho_G(Z)$, after different polymerization time at $\sigma_i = 0.508$ and $P_r = 0.005$. (See Figure 5.) Here we choose a fast polymerization rate and a relatively large initiator density so that we can observe an obvious growth of the film. As shown in the Figure, in the early stage of the reaction, a thin film very near to the surface is almost occupied by the grafted monomers. As the polymerization continues, the region with saturated graft density expands toward the top wall, showing the dynamic growth process of the film.

To study the influence of the initiator density on the film growth, we plot $\rho_G(Z)$ with different σ_i after the same process of polymerization ($P_r = 0.002$ and 5000 time units). (See Figure 6a.) All of the curves are similar in that they suddenly rise near the surface and then decay gradually to zero. It is clear that the systems with higher initiator density show a larger graft density value in the direction perpendicular to the wall. This result can be easily understood that more brush chains can grow up in the systems with higher initiator densities, and thus more free monomers can be grafted in these systems. The slightly higher density than the global value of $\rho = 0.85$ near the surface is attributed to the local enrichment of grafted monomers caused by the polymerization.

If we normalize the graft density distribution presented in Figure 6a, which is divided by the number of the initiators in each system (i.e., $\bar{\rho}_G(Z) = \rho_G(Z)/N_i = \rho_G(Z)/(\sigma_i \times L_x \times L_y)$), then the result is different, as shown in Figure 6b. It can be seen that the systems with lower initiator densities now possess larger normalized graft densities. This actually reflects the initiation efficiency of the initiators with different σ_i values. The chains in the systems with higher initiator densities will compete with each other for the ambient free monomers; moreover, grown chains have to suffer the excluded volume effect between chains. As a result, the initiation efficiency in these systems is poorer than that with dilute initiators, in which the chains are nearly growing freely. It can also be reflected by the conformation of the end-tethered chains with low initiator density found in our simulations: the mushroom conformation similar to that of the free chains implies a much easier growth process.

By investigating the influence of the reaction rate on the graft density distribution along the z direction, we find that at the same σ_i value, the growth of the film is completely dependent on the rate of the polymerization. The faster polymerization process yields faster film growth, which is not an unexpected result.

3.5. Unsaturated Initiator. In Figure 7a we present the time evolution of the fraction of unsaturated initiators $f_{N=1}$ (defined by the ratio of the number of unsaturated initiators $N_i^{\text{unsaturate}}$ to the number of the total initiators N_i; that is, $f_{N=1} = N_i^{\text{unsaturate}}/N_i$, so the value of $(1 - f_{N=1})$ is the initiation efficiency). In the early stage, for the systems with the same P_r, $f_{N=1} \sim t$ curves almost coincide with each other, indicating the free polymerization stage without competition of ambient free monomers and excluded volume effect between the growing short chains. After a certain polymerization time, $f_{N=1}$ drastically decreases for the systems with $\sigma_i = 0.127$ as compared with that with $\sigma_i = 0.508$, which implies that in the latter case, the already grown chains will screen the unsaturated initiators from connecting to the monomers. It is attributed to that for higher initiator density; the monomers nearby the wall will be consumed in a short time, and the monomers far away are difficult to diffuse through the polymer brushes and react with the surface initiators. For the systems with $\sigma_i = 0.127$, we find that a larger P_r yields a faster decrease in $f_{N=1}$. It is clear that for the systems with low initiator density, the grown chains have little influence on each other because of the large distances between them. Therefore, faster polymerization (larger P_r) gives birth to more grown chains in the early stage. In the late stage, almost all of the initiators are used to grow the chains, and thus $f_{N=1}$ decreases more quickly. However, for the systems with $\sigma_i = 0.508$, the lower P_r yields a faster decrease in $f_{N=1}$. In the system with larger σ_i and larger P_r, a part of the chains can grow rapidly, consuming almost all of the free monomers near the surface. Then, these chains continuously grow to consume the free monomers far away from the surface further. As a result, the unsaturated initiators have little opportunity to contact free monomers. The fast growing chains form a screening region between the unsaturated initiators and the upper free monomers and inhibit the latter diffuse to the surface. Therefore, there is nearly no decrease in $f_{N=1}$ in the late stage for this system, as shown in Figure 7a. Nevertheless, the situation is different for the systems with slower polymerization rates. In these systems, because the polymerization rate is slow or moderate, all of the initiators have almost an

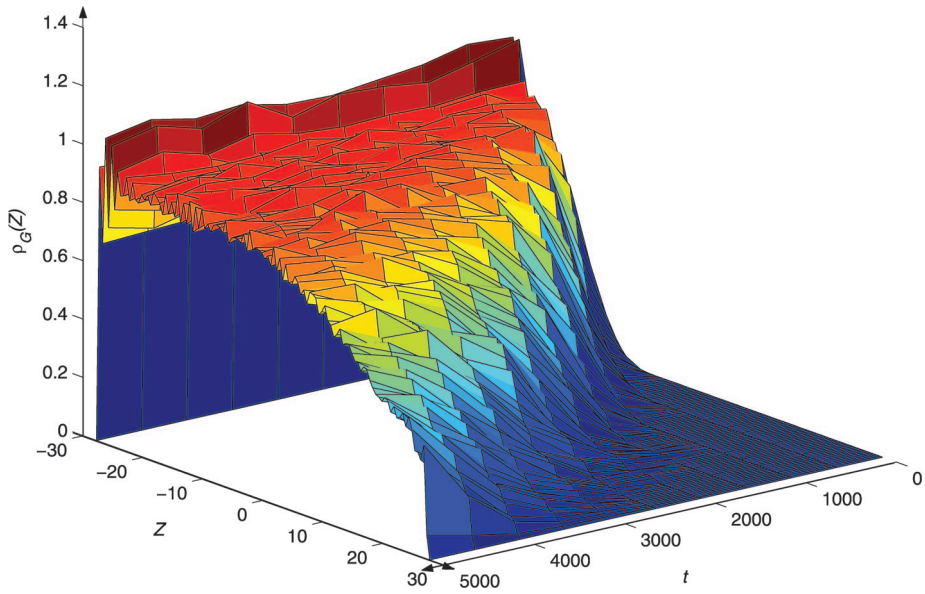

Figure 5. Graft density profile in the z direction at different polymerization time with $\sigma_i = 0.508$ and $P_r = 0.005$. Four independent samples are simulated under the same condition to calculate the mean value and the error bar. The error bars are not shown here for clarity.

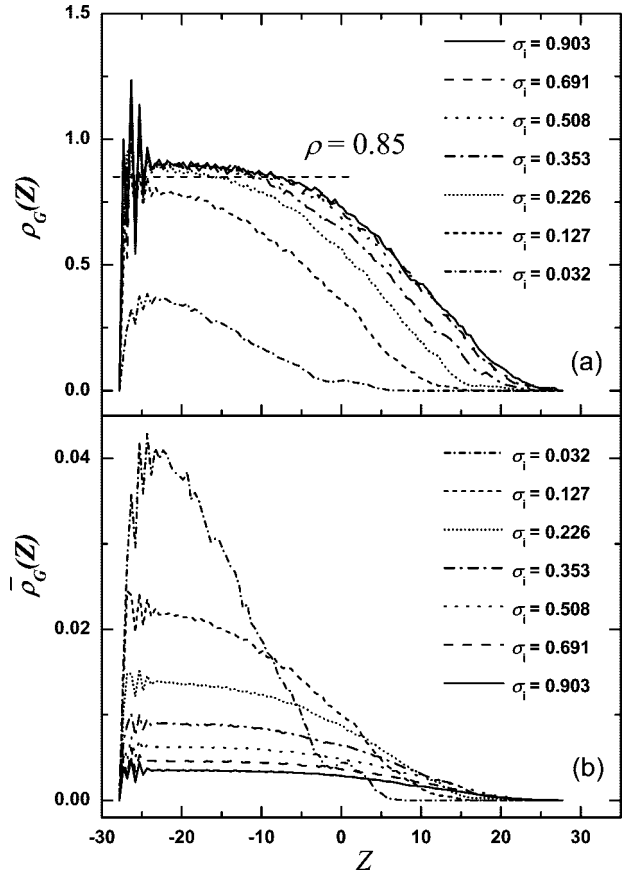

Figure 6. (a) Absolute and (b) normalized graft density profile in the z direction with different σ_i after the same process of polymerization ($P_r = 0.002$ and 5000 time units). Four independent samples are simulated under the same condition to calculate the mean value and the error bar. The error bars are not shown here for clarity.

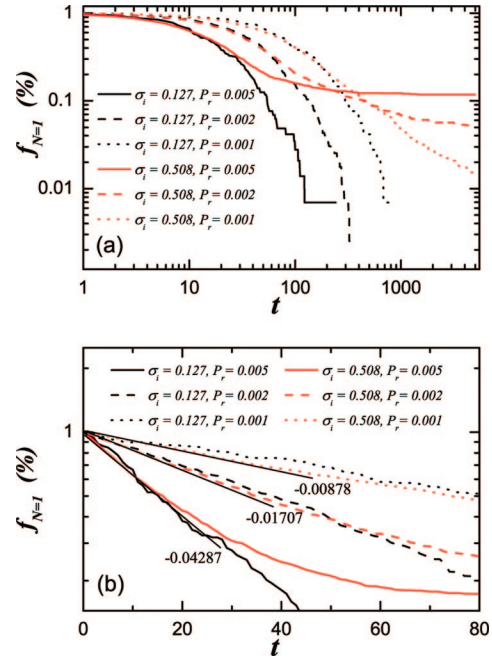

Figure 7. Time evolution of the fraction of unsaturated initiators: (a) the log−log coordinates and (b) the semilog coordinates in the early stage. The red sets denote the results of the systems with different P_r at $\sigma_i = 0.508$, and the black sets denote the results with different P_r at $\sigma_i = 0.127$.

equivalent chance of being connected, and enough monomers can diffuse into the region near the unsaturated initiators. Moreover, because the polymerization is slower, the active ends have the chance to diffuse to farther regions from the surface, leading the polymerization away from the surface. As a result, there are still many free monomers near the surface, which provide the possibility for the unsaturated initiators to be reacted later. Therefore, we find that for the systems with slow or moderate P_r, the unsaturated initiators can continue to be induced in the late stage.

With a further investigation, we replot Figure 7a in semilog coordinates, as shown in Figure 7b. Interestingly, we find a linear decay power law for $f_{N=1}$ in the early stage of polymerization. As shown in Figure 7b, at the same P_r, the curves for $\sigma_i = 0.127$ and 0.508 can both be generally fitted on the same linear decay in the early stage of polymerization. If there is no screening effect of the grown chains, then the number of unsaturated initiators, $N_i$unsaturate, after time t should be

$$N_i^{\text{unsaturate}} = N_i(1 - P_r)^k \tag{6}$$

where $k = t/(\Delta t \cdot \tau)$ is the frequency of the polymerization since the beginning of the reaction. Therefore

$$\log(f_{N=1}) = \log(N_i^{\text{unsaturate}}/N_i) = \left[\frac{\log(1 - P_r)}{(\Delta t \cdot \tau)}\right] t \tag{7}$$

For $P_r = 0.001$, 0.002, and 0.005, we can calculate the values of $[\log(1 - P_r)/(\Delta t \cdot \tau)]$ to be -8.69×10^{-3}, -1.74×10^{-2}, and -4.35×10^{-2}, respectively. From Figure 7b, we find the slopes of the decay curves in the early stage to be very close to the calculated values. Therefore, in the early stage of the polymerization, the unsaturated initiators can be considered to be "freely" induced and suffering no or little "screening effect" of the grown chains. At later time, the screening effect of the grown chains causes the number of the unsaturated initiators to decrease less sharply. The systems with higher initiator densities show especially obvious screening effects. Therefore, the curves of $\sigma_i = 0.508$ deviate from the decay line much earlier than those of $\sigma_i = 0.127$.

3.6. Bond Orientation and Chain Stretch. In the simulations, the average bond orientation can be characterized by the second Legendre polynomial, $P_2(\cos\theta)$. Because of the repulsion from the wall and the excluded volume effect, the chains are stretched more or less in the direction normal to the wall. The chain stretching can also be reflected by the bond orientation function $P_2(\cos\theta)$ for a bond with index, n, which is defined as the bond between monomer n and $n + 1$ in the polymer brush chain. Figure 8 shows the bond orientation function $P_2(\cos\theta_n)$ with bond index n for the system with $\sigma_i = 0.903$ and $P_r = 0.001$. As shown in Figure 8, when the bond index n is small, the bond orientation function exhibits an obvious exponential decay. By using off-lattice Monte Carlo simulation of living polymers, Milchev et al.[53] indicated that the bond orientation function obeys the power law $P_2(\cos\theta_n) \propto n^{-0.49}$. In our simulations, we also find a similar power law for short chain lengths, as clearly shown in the inset of Figure 8. When n is larger, the bonds tend to be randomly orientated in the space (corresponding to $P_2(\cos\theta_n)$ fluctuating around zero), which indicates that the chain stretching induced by the wall is absent in the region far away from the surface. However, it should be noted that the results shown in Figure 8 correspond to a system with high initiator density and slow polymerization rate. For other conditions, for example, when we choose lower σ_i or larger P_r, the scaling of -0.49 between $P_2(\cos\theta_n)$ and n disappears. Here the excluded volume effect plays an important role. For the systems with higher σ_i and smaller P_r (e.g., $\sigma_i = 0.903$ and $P_r = 0.001$ in Figure 8), we can obtain denser grafted chains than those with lower σ_i or larger P_r. Therefore, the chains have to suffer from the excluded volume effect and grow up straight because they have little space to develop in the lateral directions. For the systems with lower σ_i or larger P_r, the chains grow freely in any direction so that $P_2(\cos\theta_n)$ decays to zero very quickly with increasing n. Therefore, this -0.49 scaling is valid in the case of excluded volume effect dominating.

Besides $P_2(\cos\theta)$, the chain stretching can also be characterized by the chain stretch parameter

$$\phi_s = \frac{\langle R_g^z \rangle}{\left[\frac{1}{2}(\langle R_g^x \rangle + \langle R_g^y \rangle)\right]} \tag{8}$$

where R_g^x, R_g^y, and R_g^z denote the radius of gyration in the x, y, and z directions. For ordered distributed surface initiators, the grown chains possess similar R_g^x and R_g^y because they are symmetric. Therefore $\phi_s = 1$ corresponds to a chain with spherical coil configuration, and $\phi_s > 1$ denotes the fact that the chain generally stretches along the z direction. The value of ϕ_s indicates the degree of the chain stretching. Figure 9a shows the time evolution of ϕ_s in the cases of $P_r = 0.001$ but different σ_i. Here we choose the small polymerization rate, $P_r = 0.001$, to gain the high initiation efficiency. For the systems with low initiator densities, the value of ϕ_s is near 1, indicating that the chain configuration is roughly a spherical coil; that is, the polymer brushes possess mushroom configuration. ϕ_s increases

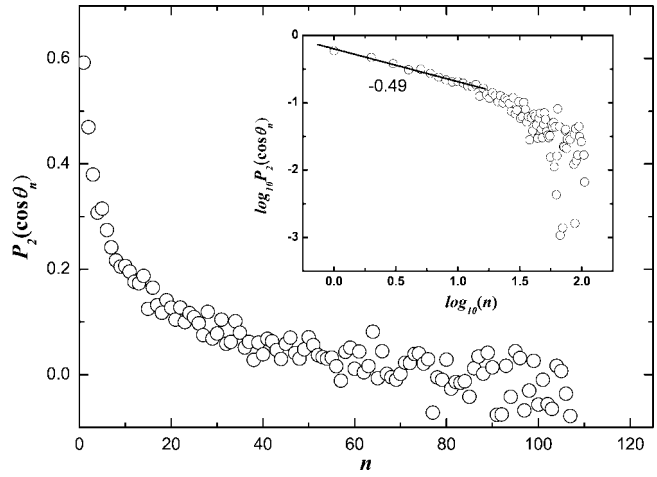

Figure 8. Bond orientation function $P_2(\cos\theta_n)$ with bond index n for the system with $\sigma_i = 0.903$ and $P_r = 0.001$. Six independent samples are simulated under the same condition to calculate the mean value and the error bar. The error bars are not shown here for clarity.

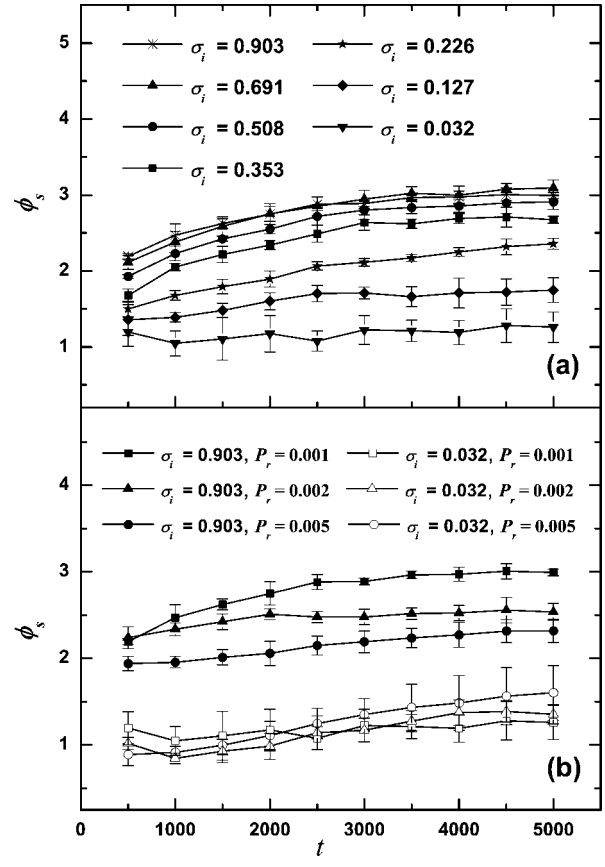

Figure 9. Time evolution of the stretch parameter ϕ_s (a) in the case of $P_r = 0.001$ but different σ_i and (b) in the case of $\sigma_i = 0.032$ and 0.903 but different P_r. Four independent samples are simulated under the same condition to calculate ϕ_s mean value and the error bar.

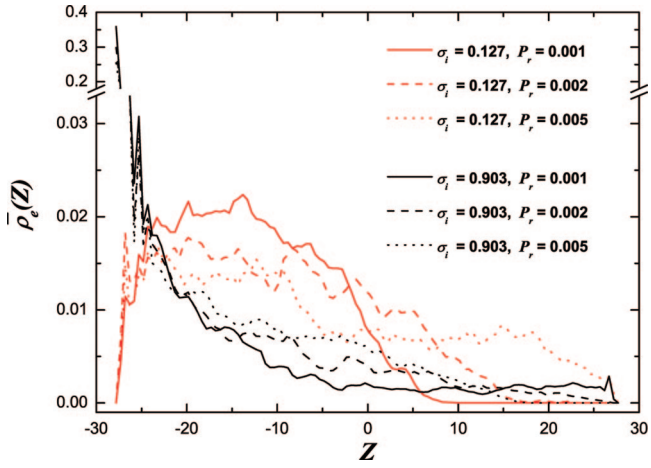

Figure 10. Normalized average active end density distribution along the z direction in the case of $\sigma_i = 0.127$ and 0.903 but different P_r. The red sets denote the systems with $\sigma_i = 0.127$, and the black sets denote $\sigma_i = 0.903$. Five independent samples, 1000 snapshots obtained in each, are simulated under the same condition to calculate the mean value and the error bar. The error bars are not shown here for clarity.

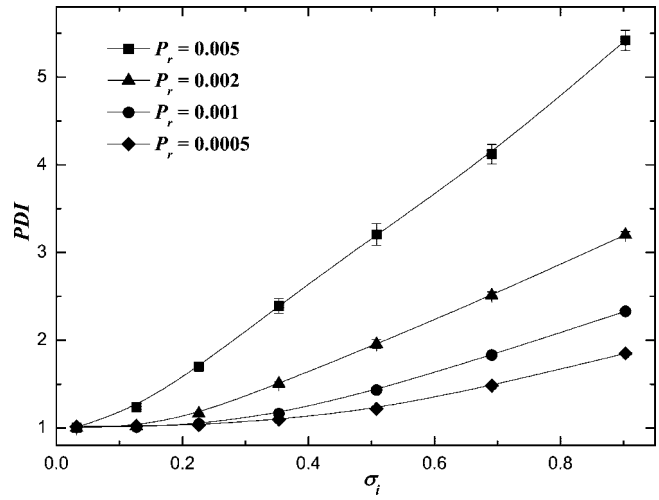

Figure 11. Variation of polydispersity index (PDI) of the grafted polymer chains with increasing σ_i at different polymerization rates. Four independent samples are simulated under the same condition to calculate PDI mean value and the error bar.

with increasing σ_i, denoting that the chains are stretched when the local environment is crowded. The systems with very high initiator densities (e.g., $\sigma_i = 0.691$ and 0.903) yield almost the same values of ϕ_s, which shows that in the two systems the local environments for the chains are similar and the chains cannot become more crowded. In almost all of the systems, the value of ϕ_s increases slightly as time elapses. This phenomenon suggests that during the chain growth process, R_g increases, and thus the excluded volume effect may further induce the stretch along the z direction.

In Figure 9b we present the comparison of ϕ_s for the systems with the same σ_i but different P_r. In the case of low initiator density with $\sigma_i = 0.032$, we can find that the three systems with different P_r values possess the similar stretch parameter, that is, $\phi_s \approx 1$. The system with $P_r = 0.005$ has a slightly larger ϕ_s in the late stage just because the chains grow faster in this system. However, in the case of high initiator density with $\sigma_i = 0.903$, we find apparent differences between systems with different P_r values. The system with $P_r = 0.001$ has the larger value of ϕ_s, and the system with $P_r = 0.005$ has the smaller value. This is simply because in the case of high initiator density $\sigma_i = 0.903$, the system with $P_r = 0.001$ has a higher initiation efficiency such that the chains are too crowded and have to stretch upward. On the contrary, the systems with faster polymerization rates have lower initiation efficiency, and the chains have enough space to diffuse laterally.

3.7. Active End Distribution. To investigate the active end distribution in the cases of different σ_i and P_r further, in Figure 10, we show the normalized average active end density distribution along the z direction $\bar{\rho}_e(Z)$ (defined as the active end density, $\rho_e(Z)$, divided by the number of initiators, N_i; that is, $\bar{\rho}_e(Z) = \rho_e(Z)/N_i$) with different σ_i and P_r. In the case of high initiator density with $\sigma_i = 0.903$, one can find more active ends in the region near the surface. However, in the case of low initiator density with $\sigma_i = 0.127$, the result is on the contrary. As we explained above, because of the screening effect of the grown chains on the unsaturated initiators, the initiation efficiency is always low in the systems with high σ_i. Therefore, there is a large fraction of unsaturated initiators in the case of $\sigma_i = 0.903$ as a result of the low initiation efficiency. Therefore, we find a fairly concentrated distribution of active ends near the surface when $\sigma_i = 0.903$. In comparison, $\sigma_i = 0.127$ is lower than the critical value of initiator density, as presented in Figure 4a, so the initiation efficiency is high. Almost all of the initiators can grow up into chains in the systems with $\sigma_i = 0.127$, and thus the active ends can distribute everywhere along the z direction. This result is completely different from the simulation results with monodisperse polymer brush model, for example, figure 4 in ref 2, in which they obtained a near-Gaussian active end distribution. This is because they have not taken the influence of the polymerization process into consideration.

3.8. Polydispersity and Mass Distribution. A very important parameter for the growth of polymer brushes is the polydispersity index (PDI), where

$$\mathrm{PDI} = \frac{\bar{M}_w}{\bar{M}_n} = \frac{\sum_i N_i M_i^2 / \sum_i N_i M_i}{\sum_i N_i M_i / \sum_i N_i} \tag{9}$$

We present the mean values of PDI for each system with different σ_i and P_r in Figure 11. At the same P_r, PDI of the grafted chains increases with increasing initiator density. When σ_i is very low, PDI is a little larger than 1.0, indicating a homogeneous growth process of the chains. When σ_i increases to larger values, PDI increases sharply, implying the emergence of the screening effect of the grown chains, which leads to the contrast of the growth conditions of short and long chains. At the same initiator density, the systems with faster polymerization possess a larger PDI, which supports the fact that a serious screening effect of the grown chains occurs in such systems. If σ_i and P_r are simultaneously high, then a large part of the initiators have to remain unsaturated ($N = 1$) or to grow to very short chains. Therefore, it can be expected to obtain a very large value of PDI in such systems. According to the results concerned, if one needs to keep the polydispersity of high density brushes as low as possible, then the surface polymerization rate should be kept as slow as possible. A relatively homogeneous growth condition of the chains would profit the occurrence of low dispersity.

Here we further compare our results with available experimental data. Devaux et al.[70] had achieved very high graft density (1.10 chain/nm^2) of the polystyrene chains grown on the silicon surface at fairly low polydispersity (PDI $\approx$ 1.1). According to the molar mass (104.15 g/mol) and the density (0.909 g/cm^3) of styrene, we can roughly calculate that the diameter of a "coarse-grained" styrene bead is 7.14 Å. If we normalize the diameter to be 1, then we can find that the reduced graft density

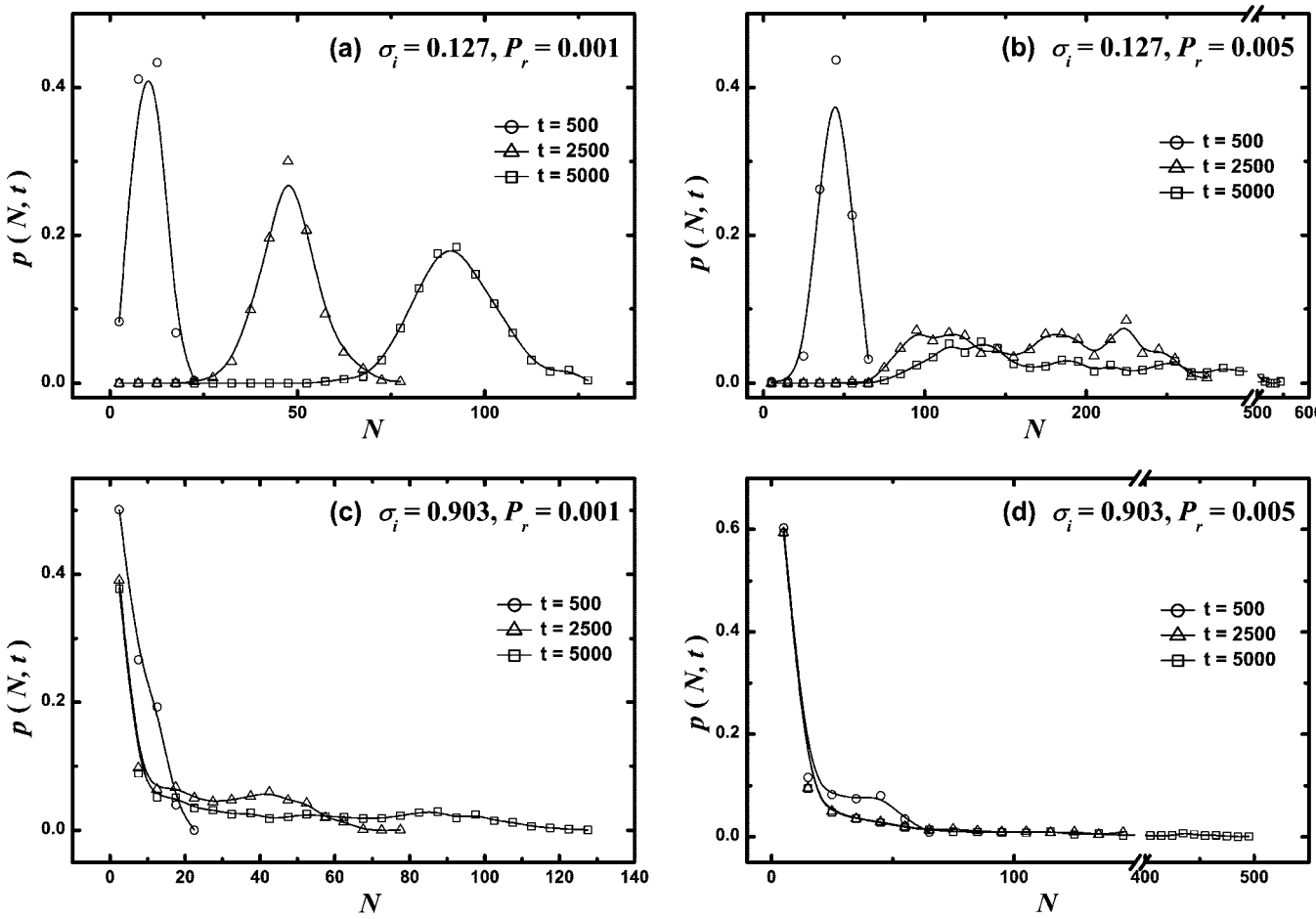

Figure 12. Mass distribution $p(N, t)$ at different times after the start of polymerization in the systems with different σ_i and P_r.

of 1.10 chain/nm^2 should be 0.56 in reduced unit in our model. Because the unsaturated initiators are considered to be the chains with length $N = 1$ in the calculation of PDI, here the initiator density, σ_i, and the so-called "graft density" could be considered to be equivalent. (Note that the concept "graft density" in ref 70 means the density of the really initiated chains in unity area, which is not the same as that in our article.) Therefore, we can have a reasonable comparison between the experimental results and the current simulation. From Figure 11, we find that the value should be PDI = 1.27 at $\sigma_i = 0.56$ when $P_r = 0.0005$, which is a little larger than the experimental result (PDI = 1.10). Because faster reaction rates correspond to larger values of PDI, if we further decrease the polymerization rate, then a PDI value close to 1.10 can be expected to be obtained.

Figure 12 shows the mass distribution $p(N, t)$ at different times after the start of polymerization in the systems with different σ_i and P_r. In the case of low initiator density and slow reaction rate (Figure 12a), we can find the mass distribution to be Poisson-like, implying the competition-absent growth like the free chains. When the initiator density is low but the reaction rate is fast (Figure 12b), $p(N, t)$ is still Poisson-like in the beginning of the polymerization. However, the fast chain growth leads to screening effect and great chain length difference. Therefore, the Poisson-like shape of $p(N, t)$ is replaced by a much broader distribution. In the case of high initiator density (Figure 12c,d), the initiation efficiency is the dominant factor, showing an extremely high distribution of the mass near $N = 1$ ($N = 1$ corresponds to the unsaturated initiators). It should be noted that $\sigma_i = 0.903$ corresponds to the limit condition compared with experiments. The very high graft density in ref 70 of 1.10 chain/nm^2 corresponds to 0.56 in our model. We find that the first value of $p(N, t)$ in Figure 12c is smaller than that in Figure 12d, which implies fewer unsaturated initiators in this system, that is, higher initiation efficiency when P_r is small. This conclusion agrees with that in Section 3.5. Furthermore, we find no difference between the first values of $p(N, t)$ in Figure 12d at different times, which indicates the strong screening effect of the fast grown chains. Figure 12c,d has low distribution at the region of large chain lengths. This result can be easily understood. In the system with high σ_i, the small part of surviving chains from the competition of the growth near the grafting plane obviously has less hindrance to grow longer and longer. Therefore, we can find a broad distribution of the chains as the chain length increases.

4. Conclusions

In this study, the surface-initiated polymerization with different initiator densities and polymerization rates has been investigated using MD simulations. By characterizing the time evolution of the distance between the center of mass of the grafted monomers and the grafting plane, we find that it is necessary to choose slow-to-moderate reaction rates in the model to keep it a controllable living polymerization. We then study the variation of the grafted monomer fraction, f_G, with increasing σ_i at different polymerization rates. In agreement with the experimental results, we obtain a window of σ_i as the critical value of the initiation efficiency. When the initiator density is lower than the critical value, the initiation efficiency is nearly 100%. In particular, the graft density profile in the z direction, whose variation reflects the growth of the polymer film, is studied. By comparing the absolute and normalized graft densities along the z direction of different systems, we find that when initiator density is low, the initiation efficiency is always

high. However, in the systems with high initiator density, the slow or moderate polymerization yields relatively higher initiation efficiency. Moreover, the time evolution of the fraction of unsaturated initiators is characterized. We find a screening effect of the grown chains on the unsaturated initiators when the initiator density is high, which may be one of the main reasons that causes universal low initiation efficiency in the systems with high initiator density. We have also studied the bond orientation function $P_2(\cos\theta_n)$ with the bond index, n, and the time evolution of the chain stretch parameter, ϕ_s. We find that the conformation of the chains mainly depends on the excluded volume effect. Therefore, the systems with dilute chains commonly possess mushroom configuration, and the systems with densely grafted chains are often obliged to stretch along the surface normal direction. The -0.49 scaling between $P_2(\cos\theta_n)$ and t, characterizing the excluded volume effect, is found also dependent on the polymerization rate. The normalized active end density distribution is also investigated, and broader chain end distribution is obtained than that in the monodisperse polymer brushes. Besides, the observed fairly concentrated distribution of unsaturated initiators near the surface again implies the screening effect of the grown chains on the unsaturated initiators. Moreover, the influences of σ_i and P_r on the polydispersity as well as the mass distribution of the grown chains are especially investigated. A relatively slow polymerization and low initiator density will profit the occurrence of low dispersity and narrow mass distribution.

In this study, we find that the properties of the polymer brushes are greatly dependent on the coupling between the initiator density and the polymerization rate. The excluded volume effect also plays a crucial role in the system, especially when the chains are densely grafted. By tuning the initiator density and modifying the polymerization rate, we can obtain the polymer brushes with different degrees of polydispersity. This study partially emphasizes the importance of considering the effects of polymerization rate in further investigations.

Acknowledgment. This work is supported by the National Science Foundation of China (20774036, 50803002) and Fok Ying Tung Education Foundation (114018).

References and Notes

(1) Pal, S.; Seidel, C. *Macromol. Theory Simul.* **2006**, *15*, 668.
(2) Chen, C.-M.; Fwu, Y.-A. *Phys. Rev. E* **2000**, *63*, 011506.
(3) Goujon, F.; Malfreyt, P.; Tildesley, D. J. *Chem. Phys. Chem.* **2004**, *5*, 457.
(4) Malfreyt, P.; Tildesely, D. J. *Langmuir* **2000**, *16*, 4732.
(5) Pastorino, C.; Binder, K.; Kreer, T.; Mller, M. *J. Chem. Phys.* **2006**, *124*, 064902.
(6) Advincula, R. *Adv. Polym. Sci.* **2006**, *197*, 107.
(7) Prucker, O.; Rühe, J. *Macromolecules* **1998**, *31*, 592.
(8) Jordan, R.; Ulman, A. *J. Am. Chem. Soc.* **1998**, *120*, 243.
(9) Weck, M.; Jackiw, J. J.; Rossi, R. R.; Weiss, P. S.; Grubbs, R. H. *J. Am. Chem. Soc.* **1999**, *121*, 4088.
(10) Yamamoto, S.; Tsujii, Y.; Fukuda, T. *Macromolecules* **2000**, *33*, 5995.
(11) Jones, D. M.; Brown, A. A.; Huck, W. T. S. *Langmuir* **2002**, *18*, 1265.
(12) Ejaz, M.; Yamamoto, S.; Ohno, K.; Tsujii, Y.; Fukuda, T. *Macromolecules* **1998**, *31*, 5934.
(13) Kong, X.-X.; Kawai, T.; Abe, J.; Iyoda, T. *Macromolecules* **2001**, *34*, 1837.
(14) von Werne, T.; Patten, T. E. *J. Am. Chem. Soc.* **2001**, *123*, 7497.
(15) Husseman, M.; Malmstrm, E. E.; McNamara, M.; Mate, M.; Mecerreyes, D.; Benoit, D. G.; Hedrick, J. L.; Mansky, P.; Huang, E.; Russell, T. P.; Hawker, C. J. *Macromolecules* **1999**, *32*, 1424.
(16) Zhou, Q.; Nakamura, Y.; Inaoka, S.; Park, M.; Wang, Y.; Mays, J.; Advincula, R. *PMSE [Prepr.]* **2000**, *82*, 291.
(17) Baum, M.; Brittain, W. J. *Macromolecules* **2002**, *35*, 610.
(18) Sedjo, R. A.; Mirous, B. K.; Brittain, W. J. *Macromolecules* **2000**, *33*, 1492.
(19) Alexander, S. *J. Phys. (Paris)* **1977**, *38*, 983.
(20) de Gennes, P. G. *Macromolecules* **1980**, *13*, 1069.
(21) de Gennes, P. G. *Adv. Colloid Interface Sci.* **1987**, *27*, 189.
(22) Milner, S. T.; Witten, T. A.; Cates, M. E. *Macromolecules* **1988**, *21*, 2610.
(23) Milner, S. T. *Science* **1991**, *251*, 905.
(24) Kuznetsov, D. V.; Chen, Z.-Y. *J. Chem. Phys.* **1998**, *109*, 7017.
(25) Irfachsyad, D.; Tildesley, D.; Malfreyt, P. *Phys. Chem. Chem. Phys.* **2002**, *4*, 3008.
(26) Wijmans, C. M.; Smit, B. *Macromolecules* **2002**, *35*, 7138.
(27) Murat, M.; Grest, G. S. *Phys. Rev. Lett.* **1989**, *63*, 1074.
(28) Dickman, R.; Anderson, P. E. *J. Chem. Phys.* **1993**, *99*, 3112.
(29) Lai, P.-Y.; Zhulina, E. B. *Macromolecules* **1992**, *25*, 5201.
(30) Lai, P.-Y.; Binder, K. *J. Chem. Phys.* **1993**, *98*, 2366.
(31) Lai, P.-Y.; Binder, K. *J. Chem. Phys.* **1991**, *95*, 9288.
(32) Lai, P.-Y.; Binder, K. *J. Chem. Phys.* **1992**, *97*, 586.
(33) Grest, G. S. *J. Chem. Phys.* **1996**, *105*, 5532.
(34) Doyle, P. S.; Shaqfeh, E. S. G.; Gast, A. P. *Macromolecules* **1998**, *31*, 5474.
(35) Daoulas, K. C.; Terzis, A. F.; Mavrantzas, V. G. *J. Chem. Phys.* **2002**, *116*, 11028.
(36) Laradji, M.; Guo, H.; Zuckermann, M. J. *Phys. Rev. E* **1994**, *49*, 3199.
(37) Karim, A.; Satija, S. K.; Douglas, J. F.; Ankner, J. F.; Fetters, L. J. *Phys. Rev. Lett.* **1994**, *73*, 3407.
(38) Hu, T.-J.; Wu, C. *Phys. Rev. Lett.* **1999**, *83*, 4105.
(39) Hadziioannou, G.; Patel, S.; Granick, S.; Tirrell, M. *J. Am. Chem. Soc.* **1986**, *108*, 2869.
(40) Taunton, H. J.; Toprakcioglu, C.; Fetters, L. J.; Klein, J. *Nature* **1988**, *332*, 712.
(41) Taunton, H. J.; Toprakcioglu, C.; Fetters, L. J.; Klein, J. *Macromolecules* **1990**, *23*, 571.
(42) Cosgrove, T. *J. Chem. Soc., Faraday Trans.* **1990**, *86*, 1323.
(43) Auroy, P.; Auvray, L.; Léger, L. *Phys. Rev. Lett.* **1991**, *66*, 719.
(44) Patel, S.; Tirrell, M. *Annu. Rev. Phys. Chem.* **1989**, *40*, 597.
(45) Yamamoto, S.; Ejaz, M.; Tsujii, Y.; Fukuda, T. *Macromolecules* **2000**, *33*, 5608.
(46) Ma, H.-W.; Hyun, J.-H.; Stiller, P.; Chilkoti, A. *Adv. Mater.* **2004**, *16*, 338.
(47) Halperin, A.; Tirrell, M.; Lodge, T. P. *Adv. Polym. Sci.* **1992**, *100*, 31.
(48) Kawaguchi, M.; Takahashi, A. *Adv. Colloid Interface Sci.* **1992**, *37*, 219.
(49) Lai, P.-Y.; Halperin, A. *Macromolecules* **1991**, *24*, 4981.
(50) Prucker, O.; Rühe, J. *Langmuir* **1998**, *14*, 6893.
(51) Wittmer, J. P.; Cates, M. E.; Johner, A.; Turner, M. E. *Europhys. Lett.* **1996**, *33*, 397.
(52) Matyjaszewski, K.; Miller, P. J.; Shukla, N.; Immaraporn, B.; Gelman, A.; Luokala, B. B.; Siclovan, T. M.; Kickelbick, G.; Vallant, T.; Hoffmann, H.; Pakula, T. *Macromolecules* **1999**, *32*, 8716.
(53) Milchev, A.; Wittmer, J. P.; Landau, D. P. *J. Chem. Phys.* **2000**, *112*, 1606.
(54) Xiao, D.-Q.; Wirth, M. J. *Macromolecules* **2002**, *35*, 2919.
(55) Kim, J. B.; Huang, W.-X.; Miller, M. D.; Baker, G. L.; Bruening, M. L. *J. Polym. Sci., Part A: Polym. Chem.* **2003**, *41*, 386.
(56) Weeks, J. D.; Chandler, D.; Andersen, H. C. *J. Chem. Phys.* **1971**, *54*, 5237.
(57) Bird, R. B.; Armstrong, R. C.; Hassager, O. *Dynamics of Polymeric Liquids*; Wiley: New York, 1977; Vols. 1 and 2.
(58) Kremer, K.; Grest, G. S. *J. Chem. Phys.* **1990**, *92*, 5057.
(59) Nikunen, P.; Vattulainen, I.; Karttunen, M. *Phys. Rev. E* **2007**, *75*, 036713.
(60) Liu, H.; Xue, Y.-H.; Qian, H.-J.; Lu, Z.-Y.; Sun, C.-C. *J. Chem. Phys.* **2008**, *129*, 024902.
(61) Groot, R. D.; Warren, P. B. *J. Chem. Phys.* **1997**, *107*, 4423.
(62) Español, P.; Warren, P. B. *Europhys. Lett.* **1995**, *30*, 191.
(63) Soddemann, T.; Dnweg, B.; Kremer, K. *Phys. Rev. E* **2003**, *68*, 046702.
(64) Liu, H.; Qian, H.-J.; Zhao, Y.; Lu, Z.-Y. *J. Chem. Phys.* **2007**, *127*, 144903.
(65) Akkermans, R. L. C.; Toxvaerd, S.; Briels, W. J. *J. Chem. Phys.* **1998**, *109*, 2929.
(66) Witten, T. A., Jr.; Sander, L. M. *Phys. Rev. Lett.* **1981**, *47*, 1400.
(67) Ball, R.; Nauenberg, M.; Witten, T. A., Jr. *Phys. Rev. A* **1984**, *29*, 2017.
(68) He, G.-L.; Merlitz, H.; Sommer, J.-U.; Wu, C.-X. *Macromolecules* **2007**, *40*, 6721.
(69) Tsujii, Y.; Ohno, K.; Yamamoto, S.; Goto, A.; Fukuda, T. *Adv. Polym. Sci.* **2006**, *197*, 1.
(70) Devaux, C.; Cousin, F.; Beyou, E.; Chapel, J.-P. *Macromolecules* **2005**, *38*, 4296.

MA802817R